



**Revista
Brasileira de
Ciência do Solo**

Division – Soil in Space and Time | Commission – Soil Genesis and Morphology

Genesis and transformation of basic rock-derived soils with shiny ped faces under tropical conditions

Marcos Gervasio Pereira^{(1)*} , Rafael Cipriano da Silva⁽²⁾ , Miguel Cooper⁽³⁾ ,
Lúcia Helena Cunha dos Anjos⁽¹⁾ , Deyvid Diego Carvalho Maranhão⁽⁴⁾ and Fábio
Soares de Oliveira⁽⁵⁾

⁽¹⁾ Universidade Federal Rural do Rio de Janeiro, Departamento de Solos, Seropédica, Rio de Janeiro, Brasil.

⁽²⁾ Fundação Cearense de Meteorologia e Recursos Hídricos – FUNCEME, Fortaleza, Ceará, Brasil.

⁽³⁾ Universidade de São Paulo, Escola Superior de Agricultura “Luiz de Queiroz”, Departamento de Ciência do Solo, Piracicaba, São Paulo, Brasil.

⁽⁴⁾ Instituto de Educação, Agricultura e Ambiente – IEAA/UFAM, Humaitá, Amazonas, Brasil.

⁽⁵⁾ Universidade Federal de Minas Gerais, Departamento de Geografia, Belo Horizonte, Minas Gerais, Brasil.

ABSTRACT: Soil evolves in landscapes in a natural process in which soil properties are gradually transformed. However, the transformation of argic to ferrallic horizons in basic rock-derived soils under tropical conditions is poorly understood. Depending on the position of the soil profiles in landscape, evidence of pedogenetic transformation between different horizons might indicate the formation and destruction of aggregates with shiny faces. This study aimed to determine pedogenetic changes in basic rock-derived profiles in a toposequence, because soils derived from mafic rocks are not abundant in the study region (Pinheiral, Rio de Janeiro State, Brazil). Trenches were dug at the summit (P1), upper (P2), middle (P3), and lower (P4) thirds along the toposequence. The morphological, physical, chemical, mineralogical, and micromorphological properties of the profiles were characterized, and a weathering index was calculated from X-ray fluorescence element values. All profiles had chemical and physical properties indicating an advanced degree of weathering resulting from the parent material and tropical climate conditions. In P1 and P4 that were classified as *Nitossolos*, the most evident pedogenetic processes were ferralitization and nitidization, due to the advanced degree of weathering, accumulation of oxyhydroxides and kaolinite in the horizons, and formation of textural pedofeatures by mechanical-hydric stress and evidence of the illuviation process. Profiles P2 and P3 revealed a ferralitization process and were classified as *Latossolos*. Absence of shiny macromorphological ped faces in some Bw horizons, and their micromorphological coexistence in Bt and Bw horizons within the same profile were associated with the transformation of the blocky into a granular microstructure, suggesting argic-ferrallic horizon transformation.

Keywords: pedogenesis, soil classification, ferralitization, nitidization, textural pedofeatures.

*** Corresponding author:**

E-mail: mgervasiopereira01@gmail.com

Received: March 23, 2022

Approved: August 03, 2022

How to cite: Pereira MG, Silva RC, Cooper M, Anjos LHC, Maranhão DDC, Oliveira FS. Genesis and transformation of basic rock-derived soils with shiny ped faces under tropical conditions. Rev Bras Cienc Solo. 2022;46:e0220028.

<https://doi.org/10.36783/18069657rbcs20220028>

Editors: José Miguel Reichert and Pablo Vidal Torrado .

Copyright: This is an open-access article distributed under the terms of the Creative Commons Attribution License, which permits unrestricted use, distribution, and reproduction in any medium, provided that the original author and source are credited.



INTRODUCTION

Shiny ped faces on blocky structural elements can be regarded as evidence of the actions of pedogenetic processes, suggesting prior or current clay dispersion and/or flocculation (Buol et al., 2011; De Wispelaere et al., 2015), the clay mineral nature of the soil, and the physical and hydric behavior of the horizons (Cooper and Vidal-Torrado, 2005; Costa et al., 2018). The main process is the eluviation and illuviation of clay, which is deposited on the walls of pores and around aggregates and coarse grains.

Macroscopic shiny ped faces is a criterion with which to identify the argic horizon of the World Reference Base for Soil Resources (WRB) (IUSS Working Group WRB, 2015) and the argillic horizon of soil taxonomy, both characterized by horizons with distinctly more clay content than the overlying horizon. However, shiny ped faces can be frequently associated with other reference soil groups (RSG), as in Nitisols, Lixisols, and Acrisols (IUSS Working Group WRB, 2015). Soil taxonomy (Soil Survey Staff, 2014a) can occur in Ultisols and Alfisols. However, in modern classifications, such as WRB and soil taxonomy, shiny ped faces do not exclude the occurrence of other processes such as ferralitization. Thus, in the WRB, for example, argic can coexist with a ferralic horizon in the same profile. However, in the Brazilian System of Soil Classification (SiBCS), macroscopic shiny ped faces are important and serve as a criterion with which to distinguish types of horizons such as nítico and textural and soil classes such as *Nitossolos* and *Argissolos*, respectively (Santos et al., 2018).

Shiny ped faces can occur in different soil classes, thus interfering with establishing their relationships with degrees of soil development. Furthermore, despite the importance of soils with these features and their taxonomic relevance, especially in SiBCS, the scarcity of analytical data limits understanding of their genesis or destruction (De Wispelaere et al., 2015).

Soils derived from mafic and ultramafic rocks in tropical regions are generally characterized by shiny ped faces. For example, Ferralsols, Cambisols, and Acrisols associated with felsic rocks (granites and gneisses) mainly predominate in the dissected plateau areas of the eastern margin of the Brazilian coast, locally known as Mares de Morros (Brasil – Projeto RadamBrasil, 1983; Nummer et al., 2007; Santos et al., 2010). They are interspersed with soils associated with intrusions of basic rocks such as basalt, gabbro, and amphibolite. These rocks, together with the tropical climate of the Atlantic Forest biome and landforms characteristic of this region (Santos et al., 2010), are responsible for soils with properties that are different from their surroundings, including many shiny ped faces. These soils are usually classified as Nitisols with an argic horizon, but are almost always associated with Ferralsols with ferralitic horizons. The genetic relationship between them has been widely studied.

We evaluated the chemical, physical, mineralogical, and micromorphological properties of basic rock-derived soils along a toposequence in a southeast region of Rio de Janeiro State, Brazil, to understand the genesis and transformation of soils with shiny ped faces. The results helped to clarify the interplay of argic/nitic-ferralic horizons and show that the behavior of the clay fraction is an important driver of pedogenetic evolution in tropical regions.

MATERIALS AND METHODS

Location and characterization of the study area

The study area was located in the municipality of Pinheiral, in the southern region of the state of Rio de Janeiro, Brazil (Figure 1). This area is included in the Ribeirão do Cachimbal microbasin, which comprises part of the Paraíba do Sul River Basin, inside the Médio Paraíba Fluminense region. According to the Köppen classification system, the climate

is predominantly Cwa, characterized by a warm subtropical (mesothermal) climate with rain in summer and drought in winter (Alvares et al., 2013). The mean annual rainfall of approximately 1,389 mm is concentrated between March and November, whereas June and August are the driest months. The minimum and maximum mean annual temperatures are 14 and 30 °C, respectively, the relative humidity is >80 %, and the potential annual evapotranspiration is 995 mm (Portilho et al., 2011; Santos et al., 2016a, b).

The regional geology is complicated and was formed by tectonic features and lithostratigraphic units of the Paraíba do Sul Complex, composed mainly of granite and gneiss (Brasil - Projeto RadamBrasil, 1983; Nummer et al., 2007). These rocks are present in dikes and sills composed of basic rocks, mainly amphibolite, diabase, and basalt, which range in thickness from centimeters to meters and are marked by irregular contact with felsic rocks of a Precambrian crystalline basement and sedimentary rocks.

Region relief is dominated by a complex topography known as the *Mar de Morros* environment. These landforms are hills sculpted from ancient crystalline formations intensely dissected by hydric/fluvial erosion and have convex-convex and convex-concave hills expressed in mamelonar shapes known as half-oranges that occur in the landscape

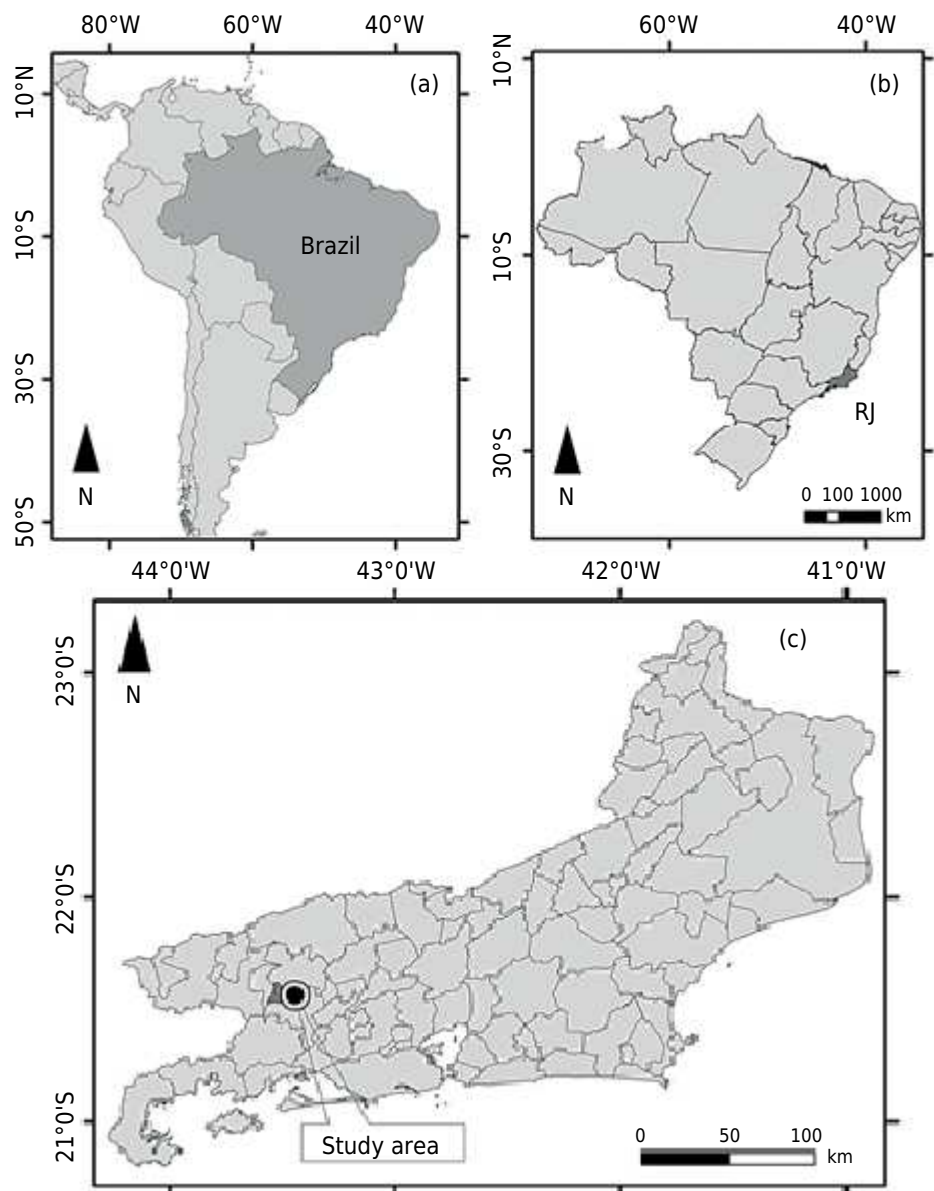


Figure 1. Localization of the studied area in Pinheiral, Rio de Janeiro State, Southeastern Brazil.

over vast homogeneous expanses. The top of *Mar de Morros* is generally flattened, constituting a watershed for small basins of existing drainage, and flat-bottomed valleys were formed from colluvial sediments (Ab'Saber, 1996).

Regional relief is defined as strong wavy to wavy prevailing areas with slopes varying from flat (0 - 3 %) to steep (>75 %) (Costa et al., 2018). Another characteristic of this region is the formation of valleys and relief features, resulting in the formation of a diversified drainage network that interferes with water dynamics in the soil and various soil properties (Fontana et al., 2014; Santos et al., 2016b; Costa et al., 2018). The mean elevation varies from 360 m above sea level (asl) in the floodplain areas of the Paraíba do Sul River to 720 m asl at the top of Serra do Arrozal (Fontana et al., 2014), whereas the elevation of the study area is 385 - 462 m asl.

Vegetation throughout the region is complex and predominates in the area the submontane semi-deciduous seasonal forest, typical of the Atlantic Forest Biome (CEIVAP, 2006). However, only 11 % of this biome's primary vegetation remains in the Paraíba do Sul River Basin, with the most expressive remnants restricted to areas with more difficult access and environmental reserves.

Toposequence selection and sample collection

Figure 2a shows a toposequence of soils derived from basic rock, probably a diabase, that we identified and characterized based on four soil profiles at various positions on the slope. The profiles were as follows: P1 (summit, 462 m; slope, 16 %; landform,

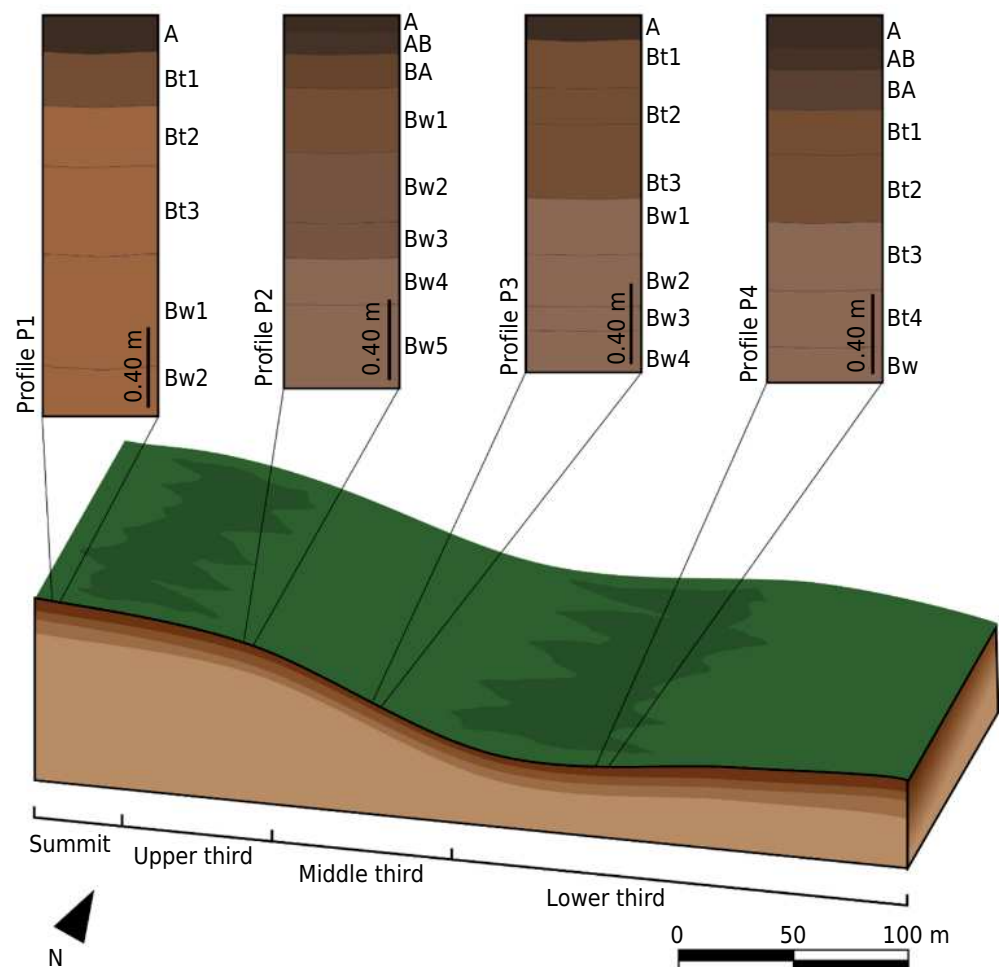


Figure 2. Schematic representation of the toposequence and soil profiles sampled in Pinheiral, Rio de Janeiro State, Southeastern Brazil.

plane without curvature), P2 (upper third, 452 m; slope, 38 %; landform, convex), P3 (middle third, 431 m; slope, 50 %; landform, plane), and P4 (lower third, 402 m; slope, 23 %; landform, aconcave). The coordinates of the profiles were: P1 (22° 32' 14.0" S; 43° 59' 56.2" W); P2 (22° 32' 11.9" S; 43° 59' 57.7" W); P3 (22° 32' 11.2" S; 43° 59' 59.4" W); P4 (22° 32' 10.8" S; 44° 00' 01.4" W).

Specific environmental conditions favor various degrees of weathering and the expression of pedogenetic processes that result in soil properties (Fontana et al., 2014). This area comprises pastures cultivated with *Brachiaria spp.*, and it shows signs of laminar and furrow erosion that indicate some degree of soil degradation.

Soil morphology of each horizon of the toposequence profiles was described according to Santos et al. (2015). Soil samples were collected, air-dried, ground, sieved through a 2-mm mesh to obtain air-dried fine earth (ADFE), and physically and chemically analyzed. We also determined soil bulk density (pb) and analyzed the micromorphology in undisturbed samples of each profile (Bullock et al., 1985; Castro and Cooper, 2019).

Laboratory analysis

We simply collected and analyzed samples. Grain size was analyzed using pipette method (Soil Survey Staff, 2014b). Fine and coarse sand, silt, and clay contents were dispersed in NaOH and measured. Water-dispersible clay contents were determined in water. Textural classes were determined from the soil textural triangle according to Santos et al. (2015), an adaptation of the classification proposed by the USDA (Soil Survey Staff, 2014b), which divides clayey soils into the distinct classes of clay and heavy clay when the clay content is $>600 \text{ g kg}^{-1}$.

Soil bulk density (pb) was determined using the metallic core method (Soil Survey Staff, 2014b; Teixeira et al., 2017) and particle density (Pd) was determined by pycnometry (Blake and Hartge, 1986; Teixeira et al., 2017). Degrees of clay flocculation (CF) were calculated from total and water-dispersible clay data.

Chemical properties were characterized using the method proposed by the Soil Survey Staff (2014b) and Teixeira et al. (2017). The pH of the soil was measured in H_2O and in KCl at a ratio of 1:2.5. Exchangeable Na and K were extracted with Mehlich-1 solution and determined by flame emission. Exchangeable Ca, Mg, and Al contents were extracted in KCl (1 mol L^{-1}) and determined by titration. We calculated cation exchange capacity ($\text{CEC} = \text{S} + \text{H} + \text{Al}$), base saturation ($\text{V\%} = \text{S} \times 100 / \text{CEC}$) and saturation by Al^{+3} ($\text{m\%} = \text{Al}^{+3} \times 100 / \text{CEC}$) (Soil Survey Staff, 2014b; Teixeira et al., 2017). Total organic carbon (TOC) was quantified by oxidation with potassium dichromate in acid medium, then titrated with a solution of ferrous ammonium sulfate (Yeomans and Bremner, 1988).

Total SiO_2 , Al_2O_3 , Fe_2O_3 , TiO_2 , CaO, MgO, K_2O , MnO, and P_2O_5 contents were determined using X-ray fluorescence (total chemical analysis). Sieved soil and undisturbed rock samples were mixed with $\text{Li}_2\text{B}_4\text{O}_7$, melted at $1,100^\circ\text{C}$ in a PERL'X3 oven and subsequently analyzed on a Magix Pro (PW-2440) spectrometer (both from Philips Nederland B.V., Eindhoven, Netherlands) with an Rh anode X-ray generator operating at 4 kw with four (200- and $750\text{-}\mu\text{Al}$, $300\text{-}\mu\text{bronze}$ and Pb) filters (Hallett and Kyle, 1993). Loss on ignition (LOI) was determined by the combustion of soil samples at $1,000^\circ\text{C}$ in a muffle furnace. Calibration curves were constructed using standard samples, and mass losses from the total oxidation of carbonates at $1,000^\circ\text{C}$ were considered. Quantitative data were analyzed using IQ+ software, and total elemental contents are expressed as ratios (%). The weight % oxide data were converted to cationic molar values, and weathering indices were calculated considering the relative accumulation of Fe and Al (RA%), and losses in silica ($\Delta 4\text{Si\%}$; Equation 2) to estimate weathering intensity expressed as ratios (%) (Meunier et al., 2013; Caner et al., 2014):

$$RA\% = R3^+ \times 100 / (R3^+ + R2^+ + M^+) \quad \text{Eq. 1}$$

in which: M^+ represents $K^+ + 2Ca^{2+}$, $R2^+$ represents $Fe^{2+} + Mg^{2+}$, and $R3^+$ represents $Al_2O_3 + Fe_2O_3$. High ratios indicate Fe and Al accumulation into oxyhydroxides such as goethite, hematite, and gibbsite (Meunier et al., 2013).

$$\Delta 4Si\% = [(4Si\%_{uw} - 4Si\%_w) / (100 - 4Si\%_{uw})] \times 100 \quad \text{Eq. 2}$$

in which: $4Si\%_{uw}$ is the Si of parent unweathered matter, $4Si\%_w$ is weathered soil samples, $4Si$ is the Si content (mmol)/4, and $4Si\%$ is $4Si \times 100 / (4Si + R2^+ + M^+)$. High $\Delta 4Si\%$ is associated with intense silicate weathering and transformation into clay minerals, with values near 100 % indicating predominant kaolinite (Caner et al., 2014).

Iron oxides were determined by extraction with sodium dithionite-citrate-bicarbonate to quantify total and low-crystallinity forms (Fe_d) (Mehra and Jackson, 1960), the latter of which was measured after extraction with ammonium oxalate (Fe_o) (McKeague and Day, 1966). Iron concentrations in the extracts were determined by atomic absorption spectrometry. The total Fe content in the soil samples ($g\ kg^{-1}$) was recalculated and converted based on X-ray fluorescence (Fe_2O_3) results multiplied by 0.7.

Soil samples from the profile horizons were mineralogically characterized by X-ray diffraction (XRD) using an model D8 Advance AXS diffractometer (Bruker Biospin Corp., Billerica, MA, USA) operating with Cu K α radiation at 45 kV, 40 mA, and $1^\circ\ 2\theta$ per minute ($0.04^\circ\ s^{-1}$) scan amplitude. These soil samples were dispersed and sedimented in NaOH $1\ mol\ L^{-1}$, then clay fractions were determined in total clay suspensions mounted on oriented slides without eliminating iron oxides (Teixeira et al., 2017).

Iron oxides in some samples of subsurface horizon profiles were concentrated in NaOH $5\ mol\ L^{-1}$ (Kämpf and Schwertmann, 1982). Thereafter, the samples were mounted in powder slides, to identify iron oxides in the clay fraction, and irradiated at intervals from 2° to $50^\circ\ 2\theta$. Diffractograms were designed using Match! (Crystal Impact, Bonn Germany) and interpreted according to Brindley and Brown (1980), and the position and intensity of reflections were analyzed.

Thin sections of some of the subsurface horizons of each profile prepared from undisturbed samples were oven-dried at $35^\circ\ C$ for micromorphological analyses. The samples were embedded in a mixture of polyester resin, styrene monomer, and fluorescent pigment with methyl ethyl ketone peroxide as the catalyst to polymerize the resin (Castro and Cooper, 2019). Sequential sample blocks were dried, cut into ($5 \times 7.5\ cm$) slices $\sim 30\ \mu m$ thick and mounted on slides. The slices were described and characterized using an Axioplan microscope (Carl Zeiss AG., Oberkochen, Germany) and a Wild Stereo Microscope (Virtual Archive of Wild Heerbrugg, Gais, Switzerland) under natural and polarized light as recommended by Bullock et al. (1985) and Stoops (2003). The slides were photographed under cross-polarized (XPL; polarizer and analyzer), plane-polarized (PPL; polarizer), and inclined reflected light.

Soil profiles were classified according to the Reference Base for Soil Resources (IUSS Working Group WRB, 2015), the Soil Taxonomy (Soil Survey Staff, 2014b) and the Brazilian System of Classification (Santos et al., 2018).

RESULTS

Morphological properties

The hues 5YR and 7.5YR prevailed in the profiles, with values of 3 or 4 and chroma of 4 or 6 (moist soil). The surface horizons tended to be predominantly dark brown (7.5YR 3/4), whereas the subsurface horizons Bw and Bt ranged from strong, to reddish brown

to yellowish-red hues (Table 1). The structure was predominantly angular and subangular blocky in the Bt horizons, with fine size and moderate-to-weak development prevailing in most of them. Medium-to-very fine subangular blocky structures predominated in the Bw horizons with weak development.

Shiny ped faces were the most frequent in the Bt horizons, especially in profiles P1 and P4, ranging from common to abundant, with a predominantly moderate degree of development. Blocky structural elements with shiny ped faces ranged from a few to common in number and degree of development in profiles P2 (Bw₂, Bw₃, and Bw₄) and P3 (Bw₁ and Bw₂). The dry and wet consistencies in surface horizons tended to be harder and firmer, respectively, and strength gradually decreased with depth. The textural classes varied little from clayey to very clayey, with no textural contrast between the horizons of the profiles. A very clayey texture predominated in both Bw and Bt.

Physical properties

Clay content was slightly higher in the deep than in the surface horizons (Table 2). The predominance of clay over other granulometric fractions resulted in silt/clay ratios <0.50 (range 0.02–0.49). However, the water-dispersible clay content was the highest in the surface horizons, resulting in a gradual increase in the ratio (%) of clay flocculation (CF) with depth.

Density did not obviously vary between the profiles. The mean values of pb were 1.17 Mg m⁻³, with small variations between horizons and a tendency to decrease with depth, as found in profile P4. Mean pb in all Bt (P1 plus p4) and Bw horizons (P2 plus P3) were 1.24 and 1.07 Mg m⁻³, respectively. Conversely, the mean values of Pd were 2.82 Mg m⁻³.

Chemical properties

The mean pH was higher in water (5.2) than in KCl (4.4), resulting in ΔpH values <1.0 (Table 3). Both pH(H₂O) and pH(KCl) tended to increase from P1 (top slope) to P4 (lower third slope). Exchangeable Ca and Mg were the main cations in CEC. Considering the acidity, the content of primarily K⁺ and Na⁺ was low. The content of Al³⁺ was slightly higher, ranging from 0.1 to 1.2 cmol_c kg⁻¹, corresponding to Al saturation (m%) ranging from 1 to 65 %, with the highest values being in the Bw horizons. The mean V% was also low (34 %) and tended to increase from P1 to P4.

Mean CEC values were low (7.5 cmol_c kg⁻¹), but because of an increase in the saturation of bases and pH in the lower third of the slope, they were higher in P4 than in the other profiles. Minimum and maximum TOC content were 2.3 and 22.1 g kg⁻¹, respectively. The TOC content was high in the superficial horizon, and gradually decreased with depth in all profiles.

Mineralogical properties and chemical analysis

Clay fraction mineralogy highlighted kaolinite's predominance in all profiles' horizons, identified by reflections in *d* values predominantly near 0.720 and 0.360 nm (12° and 25° 2 hkl in planes 001 and 002, respectively; Figure 3). Wide and less intense kaolinite reflections were evident in the surface horizons of P3 and P4, whereas the intensity increased with depth. The intensity of kaolinite reflections decreased with depth in Profiles P1 and P2. Concentration and crystallinity of goethite, another mineral found in natural clays, decreased with depth in P1, whereas the intensity tended to increase with depth in P3 and P4 (Figure 3).

The Fe_d values revealed small variations that increased with depth in profiles P1, P2 (except for horizon BA), and P4 (Table 4). The mean Fe_d was 111 g kg⁻¹, whereas Fe_o was lower, with a mean of 2.0 g kg⁻¹, resulting in the Fe_o/Fe_d ratio being <1.0. The total Fe (Fe_t)

Table 1. Field morphological properties of the sampled soils in the Rio de Janeiro State, Southeastern Brazil

Horizon	Layer	Munsell Color ⁽¹⁾	Structure ⁽²⁾	Shiny ped faces ⁽³⁾	Consistency ⁽⁴⁾		Textural class ⁽⁵⁾
					Dry	Wet	
m							
Profile P1							
A	0.00-0.18	7.5YR 3/4	st, me, ab + sbk	-	v.ha	v.fi	clay
Bt1	0.18-0.45	5YR 4/4	st, vf + f, ab + sbk	co; mo	ha	fi	h.clay
Bt2	0.45-0.75	5YR 4/6	mo, f, ab + sbk	co; mo	s.ha	fri	h.clay
Bt3	0.75-1.19	5YR 4/6	mo, f, ab + sbk	ab; mo	s.ha	fri	h.clay
Bw1	1.19-1.75	7.5YR 4/6	we, f, sbk	co; mo	so	v.fri	h.clay
Bw2	1.75- 2.00	7.5YR 4/6	we, f, sbk	co; mo	s.ha	fri	clay
Profile P2							
A	0.00-0.08	7.5YR 3/4	st, f, sbk	-	ex.ha	fi	clay
AB	0.08-0.19	7.5YR 3/4	st, f + me, sbk	-	ex.ha	fi	clay
BA	0.19-0.36	7.5YR 4/4	mo, f, sbk	-	v.ha	fi	clay
Bw1	0.36-0.68	5YR 4/4	mo, vf + f, sbk	-	ha	fri	h.clay
Bw2	0.68-1.03	5YR 4/6	mo, vf + f, sbk	fe; we	s.ha	fri	h.clay
Bw3	1.03-1.21	7.5YR 4/6	we, vf, sbk	fe; we	so	v.fri	h.clay
Bw4	1.21-1.44	7.5YR 4/6	we, vf, sbk	co; we	so	v.fri	h.clay
Bw5	1.44-1.86 ⁺	7.5YR 4/6	mo, f, sbk	-	so	v.fri	h.clay
Profile P3							
A	0.00-0.12	7.5YR 3/4	st, f + me, sbk	-	ex.ha	fi	h.clay
Bt1	0.12-0.36	5YR 4/4	mo, f, sbk	co; we	v.ha	fi	h.clay
Bt2	0.36-0.54	5YR 4/4	mo, f, sbk	co; we	ha	fri	h.clay
Bt3	0.54-0.91	5YR 4/4	mo, f, sbk	-	s.ha	fri	h.clay
Bw1	0.91-1.19	7.5YR 4/6	we, me, sbk	-	s.ha	fri	h.clay
Bw2	1.19-1.45	7.5YR 4/6	we, me, sbk	-	s.ha	v.fri	h.clay
Bw3	1.45-1.57	7.5YR 4/6	we, me, sbk	-	s.ha	fri	h.clay
Bw4	1.57-1.78 ⁺	7.5YR 4/6	we, me, sbk	-	s.ha	fri	h.clay
Profile P4							
A	0.00-0.16	7.5YR 3/4	st, vf + f, sbk	-	ex.ha	fi	clay
AB	0.16-0.27	7.5YR 3/4	st, vf + f, sbk	-	v.ha	fi	clay
BA	0.27-0.47	5YR 4/4	mo, f, sbk	co; we	v.ha	fri	clay
Bt1	0.47-0.69	5YR 4/4	mo, f, sbk	co; mo	ha	fri	h.clay
Bt2	0.69-1.03	5YR 4/6	mo, f, sbk	co; mo	ha	fri	h.clay
Bt3	1.03-1.37	7.5YR 4/4	mo, f, sbk	ab; mo	ha	fri	h.clay
Bt4	1.37-1.65	7.5YR 4/6	mo, f, sbk	ab; mo	ha	fri	h.clay
Bw	1.65-1.83 ⁺	7.5YR 4/6	we, f, sbk	ab; mo	ha	fri	h.clay

⁽¹⁾ Moist condition color. ⁽²⁾ we: weak; mo: moderate; st: strong; vf: very fine; f: fine; me: medium; ab: angular blocky; sbk: subangular blocky.

⁽³⁾ fe: few; co: common; ab: abundant. ⁽⁴⁾ so: soft; s.ha: slightly hard; ha: hard; v.ha: very hard; ex.ha: extremely hard; v.fri: very friable; fri: friable; fi: firm; v.fi: very firm; ex.fi: extremely firm. ⁽⁵⁾ Soil textural triangle according to Santos et al. (2015); h.clay: heavy clayey.

associated with other Fe phases was higher than Fe_d and Fe_o , which also resulted in the Fe_d/Fe_t ratio usually being <1.0 (mean, 0.79). The Fe_d/Fe_t ratio was >1.0 , particularly in deep horizons. The $Fe_t/clay$ ratio ranged from 0.17 to 0.34, indicating the contribution of Fe oxides to the composition of the clay fraction.

Figure 4 shows that goethite was the main iron oxide in all profiles ($d = 0.415$, 0.240 , and 0.218 nm; 21° ; 37° and 41° 2 hkl, respectively), followed by hematite ($d = 0.370$,

0.270, and 0.170 nm; 24°; 33° and 54° 2 hkl, respectively) and ilmenite ($d = 0.188$ and 0.147 nm; 48° and 63° 2 hkl, respectively). The intensity of all oxides varied between profiles and with depth, and the occurrence of oxides did not significantly differ between the Bw and Bt horizons. Reflection near 14° was attributed to kaolinite in P3 and P4. The presence of both minerals indicated difficulties in removing phyllosilicates after dispersion in NaOH 5 mol L⁻¹ (Figures 4b, 4c and 4d). No reflections were associated with gibbsite.

Table 2. Physical properties of the sampled soils in the Rio de Janeiro State, Southeastern Brazil

Horizon	Sand		Silt	Clay		FC ⁽²⁾	Silt/Clay	pb ⁽³⁾	Pd ⁽⁴⁾
	Coarse	Fine		Total	Nat ⁽¹⁾				
			g kg ⁻¹			%	Mg m ⁻³		
Profile P1									
A	180	128	174	518	359	31	0.34	0.99	2.65
Bt1	133	112	125	630	6	99	0.20	1.25	2.86
Bt2	93	83	78	746	0	100	0.10	1.20	2.87
Bt3	100	78	75	747	1	100	0.10	1.25	2.86
Bw1	98	82	79	741	28	96	0.11	1.16	2.90
Bw2	88	82	258	572	21	96	0.45	1.33	2.96
Profile P2									
A	150	111	154	585	381	35	0.26	1.17	2.81
AB	149	100	139	612	379	38	0.23	1.11	2.86
BA	161	107	155	577	241	58	0.27	1.25	2.65
Bw1	108	99	121	672	47	93	0.18	1.14	2.88
Bw2	94	97	86	723	6	99	0.12	0.89	2.90
Bw3	84	84	14	818	10	99	0.02	1.15	2.75
Bw4	77	78	45	800	4	99	0.06	1.08	2.81
Bw5	88	82	78	752	6	99	0.10	1.22	2.94
Profile P3									
A	149	123	132	596	343	42	0.22	1.26	2.91
Bt1	129	83	92	696	141	80	0.13	1.23	2.90
Bt2	94	74	115	717	19	97	0.16	1.23	2.86
Bt3	87	79	58	776	7	99	0.07	1.06	2.81
Bw1	96	81	199	624	23	96	0.32	0.93	2.93
Bw2	99	89	38	774	28	96	0.05	1.01	2.89
Bw3	101	84	41	774	5	99	0.05	0.95	2.74
Bw4	115	74	77	734	10	99	0.10	0.95	2.78
Profile P4									
A	164	182	201	453	294	35	0.44	1.22	2.68
AB	146	176	224	454	292	36	0.49	1.32	2.75
BA	131	165	210	494	85	83	0.43	1.35	2.79
Bt1	105	119	112	664	20	97	0.17	1.32	2.74
Bt2	85	100	124	691	14	98	0.18	1.31	2.70
Bt3	80	93	100	727	7	99	0.14	1.26	2.64
Bt4	84	100	111	705	15	98	0.16	1.36	2.86
Bw	88	81	48	783	11	99	0.06	1.11	3.00

⁽¹⁾ Nat: natural clay water-dispersible. ⁽²⁾ FC: flocculated clay degree [(total clay - natural clay) × 100 / total clay]. ⁽³⁾ pb: bulk density. ⁽⁴⁾ Pd: particle density.

Table 3. Chemical properties of the sampled soils in the Rio de Janeiro State, Southeastern Brazil

Horizon	pH (1:2.5)		$\Delta\text{pH}^{(1)}$	Ca^{2+}	Mg^{2+}	K^{+}	Na^{+}	Al^{3+}	H^{+}	$\text{CEC}^{(2)}$	$\text{V}^{(3)}$	$\text{m}^{(4)}$	$\text{TOC}^{(5)}$
	H_2O	KCl											
cmol _c kg ⁻¹											%	g kg ⁻¹	
Profile P1													
A	5.2	4.2	-1.0	1.9	2.9	0.09	0.03	0.3	5.9	11.1	45	6	18.9
Bt1	4.9	4.1	-0.8	1.1	1.2	0.03	0.02	0.5	3.7	6.5	35	18	8.3
Bt2	4.8	4.0	-0.8	0.5	1.0	0.02	0.02	0.8	4.3	6.7	23	33	5.3
Bt3	4.8	4.1	-0.7	0.5	0.6	0.01	0.02	0.4	4.4	6.0	19	27	4.1
Bw1	4.9	4.1	-0.8	0.4	0.8	0.01	0.02	0.6	4.2	6.0	21	32	3.5
Bw2	4.8	4.0	-0.8	0.0	1.2	0.02	0.02	1.0	4.1	6.3	20	43	2.3
Profile P2													
A	4.7	4.1	-0.6	1.3	1.6	0.10	0.03	0.5	6.7	10.2	30	14	18.5
AB	4.8	4.0	-0.8	0.8	1.1	0.06	0.03	0.8	6.0	8.9	23	29	12.7
BA	4.7	3.9	-0.8	0.8	0.6	0.03	0.16	0.8	5.0	7.3	20	35	12.3
Bw1	4.9	4.1	-0.8	0.6	0.5	0.03	0.04	0.3	5.0	6.6	19	21	7.6
Bw2	4.9	4.0	-0.9	0.4	0.7	0.01	0.02	0.9	4.7	6.8	17	45	5.7
Bw3	4.8	4.0	-0.8	0.6	0.3	0.01	0.02	0.9	4.9	6.7	14	47	4.9
Bw4	5.0	4.1	-0.9	0.1	0.9	0.01	0.02	0.5	4.9	6.4	15	33	4.8
Bw5	4.9	4.1	-0.8	0.5	0.5	0.01	0.01	1.1	4.6	6.7	15	52	3.7
Profile P3													
A	5.2	4.3	-0.9	1.7	2.3	0.13	0.03	0.2	6.6	10.9	38	5	21.7
Bt1	5.3	4.4	-0.9	1.3	1.5	0.02	0.02	0.2	4.0	7.0	40	7	9.7
Bt2	5.5	4.8	-0.7	1.9	1.4	0.01	0.02	0.1	3.6	7.0	48	3	6.8
Bt3	5.2	4.5	-0.7	1.5	0.8	0.01	0.01	0.2	3.8	6.3	37	8	4.9
Bw1	4.9	4.0	-0.9	0.2	0.8	0.01	0.01	1.2	4.0	6.1	16	55	3.8
Bw2	4.8	4.0	-0.8	0.2	0.4	0.01	0.01	1.2	4.8	6.7	10	63	3.8
Bw3	4.8	4.0	-0.8	0.0	0.7	0.01	0.02	1.2	4.7	6.6	11	60	3.8
Bw4	4.9	4.4	-0.5	0.0	0.6	0.01	0.01	1.1	5.0	6.7	10	61	3.7
Profile P4													
A	6.6	5.6	-1.0	5.9	3.1	0.16	0.03	0.1	2.7	11.9	77	1	22.1
AB	6.5	5.6	-0.9	5.7	2.2	0.06	0.03	0.1	3.2	11.3	71	1	10.3
BA	6.1	5.4	-0.7	3.0	1.5	0.03	0.03	0.1	3.5	8.1	56	2	5.0
Bt1	6.0	5.5	-0.5	3.5	1.5	0.02	0.02	0.1	2.6	7.6	65	2	4.8
Bt2	5.8	5.3	-0.5	2.8	2.1	0.02	0.02	0.1	2.7	7.7	64	2	2.8
Bt3	5.9	5.4	-0.5	3.1	1.6	0.02	0.02	0.1	2.3	7.0	66	2	3.0
Bt4	5.5	4.9	-0.6	2.2	1.6	0.02	0.02	0.1	2.7	6.5	58	3	2.6
Bw	4.9	4.0	-0.9	0.5	0.5	0.01	0.01	1.0	2.3	4.3	24	50	4.1

⁽¹⁾ ΔpH : $\text{pH}_{\text{KCl}} - \text{pH}_{\text{H}_2\text{O}}$. ⁽²⁾ CEC: cationic exchange capacity at pH 7.0 (S + H + Al). ⁽³⁾ V: saturation of bases ($\text{S} \times 100 / \text{T}$); ⁽⁴⁾ m: saturation of aluminum [$(\text{Al} \times 100 / \text{S})$]. ⁽⁵⁾ TOC: total organic carbon.

Table 5 shows that SiO₂ predominated among the other components, followed by Fe₂O₃ and Al₂O₃. Silicon (SiO₂), calcium (CaO), and potassium (K₂O) contents tended to decrease with depth, whereas the iron (Fe₂O₃), aluminum (Al₂O₃), titanium (TiO₂), and manganese (MnO) oxide tended to increase with depth in all profiles. The distribution of the MgO

content was irregular with depth, except in P2, where it tended to decrease. The mean concentrations of Fe_2O_3 , Al_2O_3 , and TiO_2 in the soil (23, 20, and 6.3 %, respectively) were higher than those in the rock (14, 14, and 3.6 %, respectively).

The RA% was high in all profiles (>97 %) and tended to increase from horizon A to horizon B. The averages were, respectively, 98.6 and 99.1% in the Bt (P1 and P4) and the Bw (P2 and P3) horizons. The trends in $\Delta 4\text{Si}\%$ were similar to those of RA%, with the Bt (P1 and P4) and Bw (P2 and P3) horizons averaging 90.5 and 92.8 %, respectively. The $\Delta 4\text{Si}\%$ was <90 % only in P4.

Table 4. Forms of iron extracted with dithionite-citrate-bicarbonate (Fe_d), acid oxalate (Fe_o) and total (Fe_t)⁽¹⁾ in the Rio de Janeiro State, Southeastern Brazil

Horizons	Fe_t	Fe_d	Fe_o	Fe_d/Fe_t	Fe_o/Fe_d	Fe_t/clay
g kg ⁻¹						
Profile P1						
A	137	47	3.2	0.34	0.02	0.26
Bt1	140	56	1.6	0.40	0.01	0.22
Bt2	137	65	1.4	0.47	0.01	0.18
Bt3	136	56	1.2	0.41	0.01	0.18
Bw1	141	53	1.2	0.38	0.01	0.19
Bw2	144	162	1.8	1.12	0.01	0.25
Profile P2						
A	148	59	1.0	0.40	0.01	0.25
AB	151	61	2.0	0.40	0.01	0.25
BA	148	167	3.3	1.13	0.02	0.26
Bw1	152	63	1.9	0.41	0.01	0.23
Bw2	149	90	2.2	0.60	0.01	0.21
Bw3	145	66	1.7	0.46	0.01	0.18
Bw4	143	166	1.2	1.16	0.01	0.18
Bw5	145	147	1.1	1.01	0.01	0.19
Profile P3						
A	137	125	3.2	0.92	0.02	0.23
Bt1	136	120	2.1	0.88	0.02	0.20
Bt2	134	149	1.8	1.11	0.01	0.19
Bt3	131	169	1.5	1.29	0.01	0.17
Bw1	132	114	1.1	0.87	0.01	0.21
Bw2	130	122	1.0	0.94	0.01	0.17
Bw3	132	116	1.0	0.88	0.01	0.17
Bw4	139	139	1.1	1.00	0.01	0.19
Profile P4						
A	143	85	3.2	0.60	0.02	0.32
AB	156	104	4.0	0.67	0.03	0.34
BA	145	134	4.7	0.92	0.03	0.29
Bt1	139	108	3.3	0.78	0.02	0.21
Bt2	132	141	2.1	1.07	0.02	0.19
Bt3	131	134	2.0	1.02	0.02	0.18
Bt4	136	143	1.9	1.05	0.01	0.19
Bw	145	159	1.2	1.10	0.01	0.19

⁽¹⁾ Fet: total iron content measured by X-ray fluorescence.

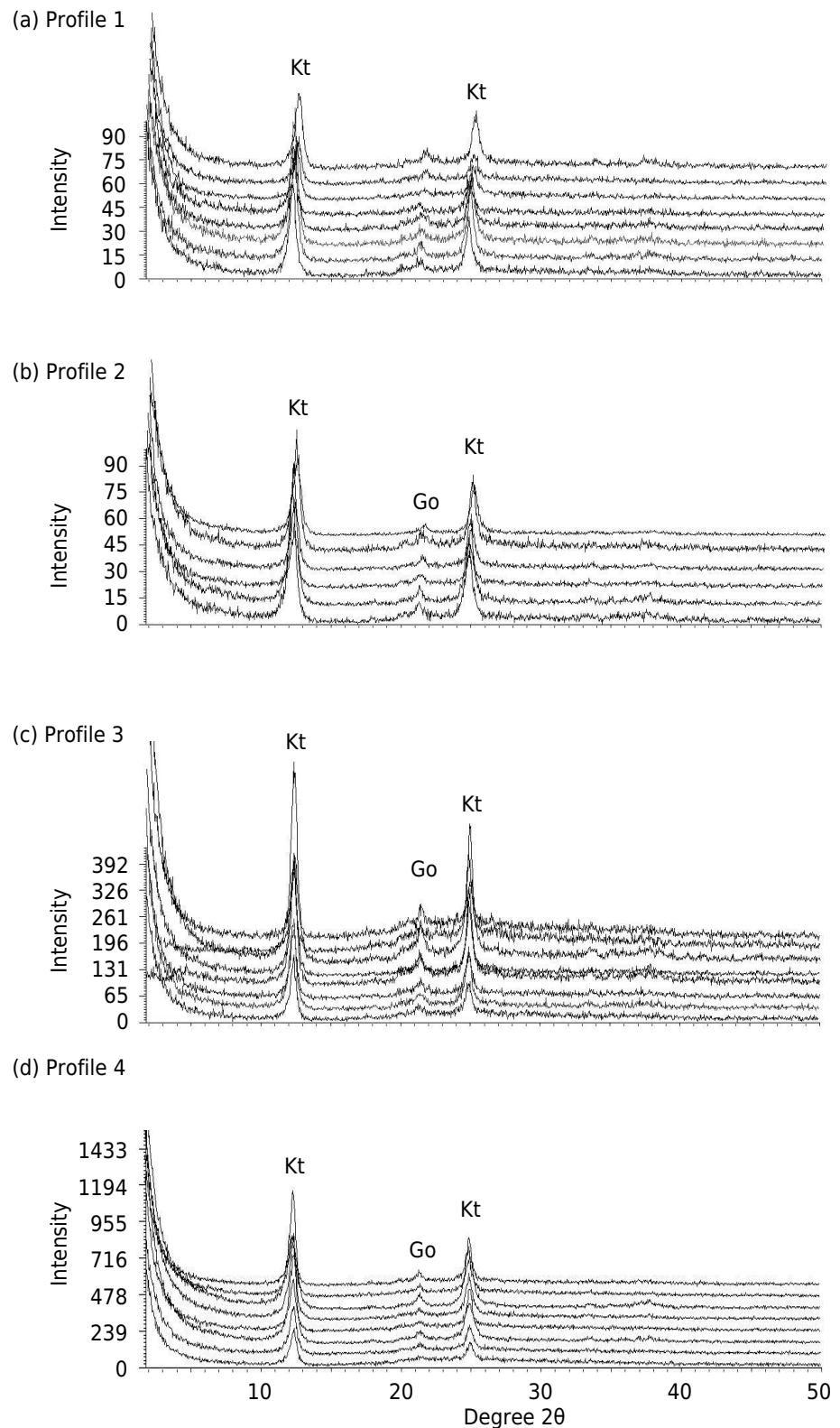


Figure 3. X-ray diffraction patterns of natural clay fraction in horizons from soil profiles located in the Rio de Janeiro State, Southeastern Brazil. Go: goethite; Kt: kaolinite.

Soil micromorphology

Microstructures in the Bt horizons were mostly angular and subangular blocky with accommodated planar voids (Table 6; Figure 5, blue arrows). Those in the Bw horizons were blocky and granular, with a compound packing void system (Table 6; Figure 6,

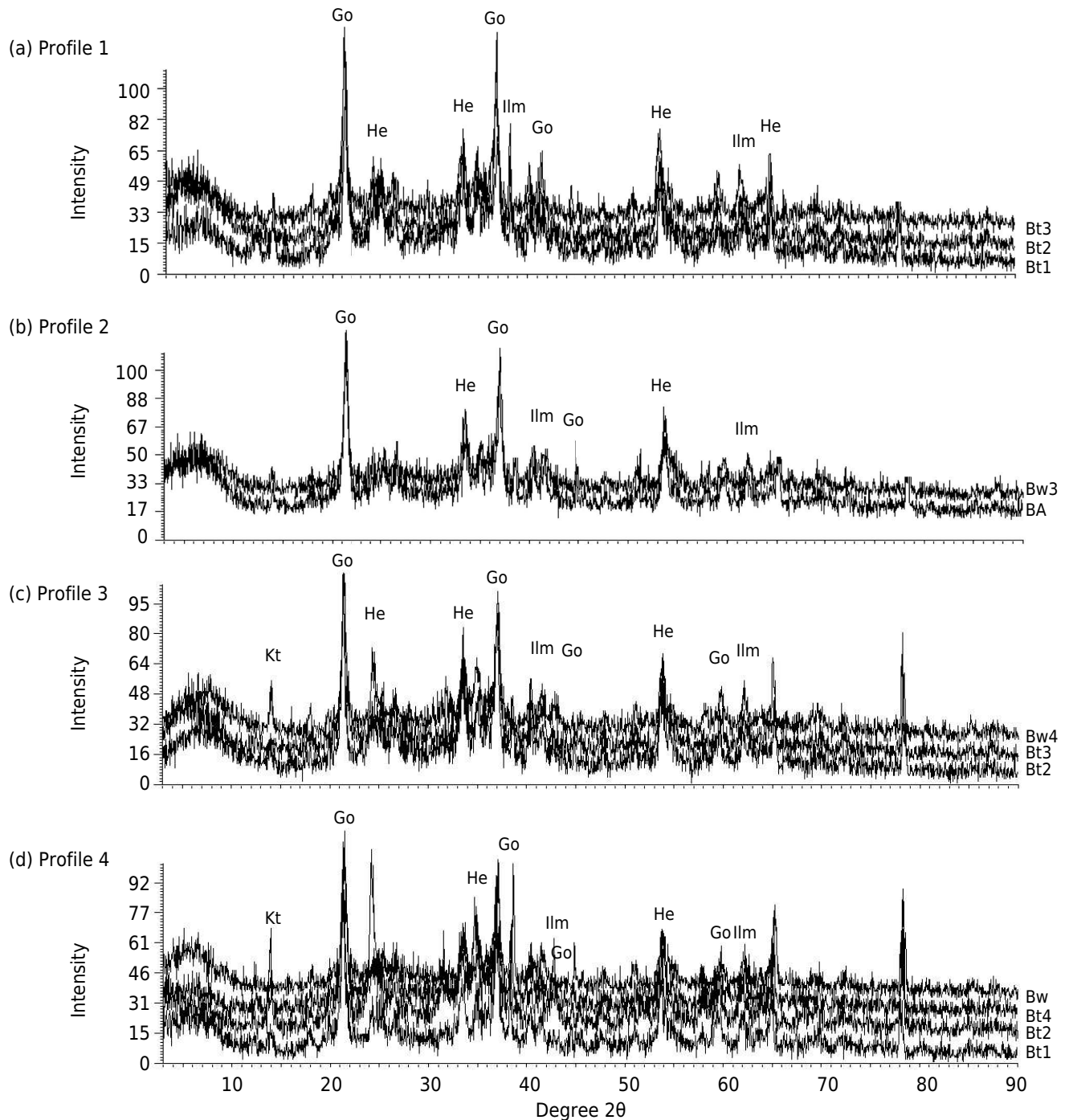


Figure 4. X-ray diffraction patterns of clay fraction (iron oxide concentration) in horizons from soil profiles located in the Rio de Janeiro State, Southeastern Brazil. Go: goethite; Kt: kaolinite.

orange arrows). Some blocks in the Bw horizon comprised coalesced granules (Figures 6e, 6f, 6g and 6h, white line).

The coarse material in the groundmass in both horizons comprised quartz, ilmenite, and magnetite grains, with low to very low frequencies of feldspar grain. In general, ilmenite and magnetite were somewhat altered, resulting in leucoxene and hematite, respectively (Figures 5 and 6, red arrows). The micromass was mostly yellowish-red and reddish yellow to strong brown in the Bt and Bw horizons, respectively. In general, the birefringence fabric (b-fabric) in the subsurface horizons (Bt and Bw) was frequently parallel-striated and stipple-speckled with strong orientation and often in large quantities. Another type of b-fabric in the horizons was mosaic-speckled and granostriated b-fabric (horizons

Bt1 and Bw2 in P1 and P2, respectively). A porphyric relative distribution prevailed in all horizons, but an enaulic relative distribution was also identified in some portions of the Bw horizon.

The main pedofeatures were textural features and nodules. Round micropeds were completely and partially coated with dense clay (Figures 5e and 5f, white arrows), voids

Table 5. Total chemical composition¹ and weathering indexes of the sampled soils and basalt rock in the Rio de Janeiro State, Southeastern Brazil

Horizon	SiO ₂	Al ₂ O ₃	Fe ₂ O ₃	TiO ₂	CaO	MgO	K ₂ O	MnO	P ₂ O ₅	Weathering indexes ⁽²⁾	
										RA%	Δ4Si%
%											
Profile P1											
A	43	17	19	6.2	0.09	0.17	0.13	0.27	0.30	97.9	89.5
Bt1	41	20	20	5.2	0.05	0.16	0.11	0.11	0.26	98.8	92.5
Bt2	39	24	20	4.7	0.03	0.15	0.11	0.07	0.27	99.1	93.3
Bt3	38	25	19	5.2	0.02	0.13	0.12	0.07	0.29	99.1	93.6
Bw1	38	25	20	7.2	0.01	0.16	0.12	0.07	0.32	99.1	93.3
Bw2	36	25	21	7.0	0.01	0.20	0.15	0.08	0.35	98.9	91.5
Profile P2											
A	37	21	21	7.0	0.06	0.17	0.08	0.13	0.38	98.8	91.6
AB	37	21	22	7.2	0.04	0.15	0.06	0.14	0.36	99.0	92.8
BA	38	20	21	7.8	0.04	0.14	0.06	0.17	0.32	98.9	92.7
Bw1	36	23	22	6.8	0.04	0.15	0.07	0.13	0.37	99.0	92.5
Bw2	37	24	21	6.2	0.03	0.15	0.07	0.09	0.37	99.2	93.5
Bw3	36	25	21	6.0	0.03	0.14	0.07	0.07	0.34	99.2	93.8
Bw4	36	25	20	6.0	0.03	0.14	0.07	0.07	0.34	99.2	93.8
Bw5	36	25	21	6.0	0.02	0.14	0.07	0.07	0.37	99.3	94.1
Profile P3											
A	39	21	20	6.9	0.08	0.15	0.08	0.15	0.37	98.7	91.6
Bt1	39	23	19	5.9	0.08	0.15	0.07	0.09	0.37	98.9	92.6
Bt2	39	24	19	5.3	0.09	0.15	0.07	0.08	0.37	98.9	92.4
Bt3	39	25	19	5.2	0.17	0.23	0.08	0.06	0.37	98.5	89.2
Bw1	39	25	19	5.5	0.03	0.13	0.08	0.06	0.37	99.2	94.4
Bw2	38	25	19	5.5	0.02	0.12	0.08	0.06	0.37	99.3	94.7
Bw3	38	25	19	5.5	0.12	0.16	0.08	0.06	0.37	98.8	91.4
Bw4	38	24	20	5.8	0.14	0.15	0.09	0.06	0.39	98.7	90.8
Profile P4											
A	40	18	20	7.3	0.39	0.23	0.18	0.37	0.38	96.2	79.2
AB	39	17	22	8.5	0.27	0.22	0.18	0.44	0.36	96.6	80.7
BA	42	18	21	8.4	0.14	0.19	0.20	0.48	0.28	97.1	84.4
Bt1	40	21	20	6.6	0.14	0.21	0.18	0.23	0.26	97.8	86.6
Bt2	38	25	19	5.4	0.11	0.20	0.17	0.14	0.31	98.4	88.2
Bt3	39	25	19	5.3	0.11	0.20	0.16	0.13	0.32	98.4	88.8
Bt4	39	24	19	5.9	0.08	0.20	0.15	0.15	0.35	98.5	89.4
Bw	37	25	21	6.1	0.03	0.15	0.07	0.07	0.37	99.2	93.8
Basalt											
Rock	51	14	14	3.6	7.9	3.5	1.94	0.17	0.62	Not applicable	

⁽¹⁾ Determined by X-Ray fluorescence. ⁽²⁾ RA: relative accumulation of iron and aluminum; Δ4Si%: relative loss of silica (Meunier et al., 2013; Caner et al., 2014).

Table 6. Micromorphological description of selected soil horizons in the Rio de Janeiro State, Southeastern Brazil

Hor ⁽¹⁾	Contexture ⁽²⁾	Relative distribution	Microstructure	Pedological features ⁽³⁾
Profile P1				
Bt1	Mosaic-speckled + granostriated + parallel striated with weak orientation; frequent.	Open porphyric	Angular and subangular blocky peds; strongly developed.	Occasional typical clay coating. Occasional typical nodules composed of iron and manganese. Rare pseudomorphs nodules of feldspar grains.
Bt2	Stipple-speckled + parallel striated with strong orientation; frequent.			Abundant typical clay coating. Occasional typical hypocoating of clay and iron. Abundant dense incomplete clay infilling. Many typical nodules composed of iron.
Bt3				Very abundant typic clay coating and iron oxides. Occasional typical hypocoating of iron oxides. Very abundant dense incomplete clay infilling. Many typical nodules composed of iron.
Profile P2				
BA	Stipple-speckled + parallel striated with strong orientation; frequent.	Open porphyric and closed enaulic	Angular and subangular blocky peds; moderately developed and granular peds.	Occasional typic clay coating and iron oxides. Occasional dense incomplete clay, silt and iron infilling. Many typical nodules composed of iron.
Bw1	Mosaic-speckled, granostriated + parallel striated with strong orientation; frequent.			Rare typic clay coating. Rare dense incomplete clay infilling. Many typical nodules composed of iron.
Bw2				Abundant typic clay coating and iron oxides. Occasional typical hypocoating. Many dense incomplete clay and iron oxides infilling. Many typical nodules composed of iron. Many papules.
Profile P3				
Bw ₁	Stipple-speckled + granostriated + parallel striated with strong orientation; frequent.	Open porphyric and closed enaulic	Angular and subangular blocky peds; moderately developed and granular peds, in some cases coalesced.	Abundant typical clay coating. Occasional typical hypocoating of iron in the interior of aggregates. Occasional dense incomplete clay infilling. Many typical nodules composed of iron.
Bw ₂				Very abundant typical clay coating. Occasional typical hypocoating of iron in the interior of aggregates. Occasional dense incomplete clay and iron oxides infilling. Many typical nodules composed of iron. Many papules.
Bw ₄				Abundant typical clay coating. Occasional typical hypocoating of iron in the interior of aggregates. Occasional dense incomplete clay and iron oxides infilling. Abundant typical nodules composed of iron. Many papules.
Profile P4				
BA	Stipple-speckled + parallel striated with strong orientation; frequent.	Double spaced porphyric	Angular and subangular blocky peds; moderately developed.	Many typical clay coating. Occasional typical hypocoating of iron oxides. Occasional dense incomplete clay and iron oxides infilling. Abundant typical nodules and concentric, composed of iron. Many papules.
Bt1	Stipple-speckled + parallel striated with strong orientation; common.	Single spaced porphyric		Very abundant typical clay coating. Abundant dense complete and incomplete clay infilling. Rare typical nodules composed of iron. Many papules.
Bt3	Stipple-speckled with strong orientation; frequent.	Double spaced porphyric		Many typical clay coating. Abundant dense incomplete clay and iron oxides infilling. Many typical nodules composed of iron.
Bt4				Many typical clay coating. Abundant dense incomplete clay and iron oxides infilling. Many typical nodules composed of iron.

⁽¹⁾ Hor: Horizons. ⁽²⁾ Contexture - frequent: 15 to 30 %; common: 30 to 50 %. ⁽³⁾ Pedological features - Rare: <2 %; occasional (2-5 %); many (5-10 %); abundant (10-20 %); very abundant (>20 %).

(Figures 5g and 5h, white arrows), and infilled voids and vughs (Figure 5f, white arrows). Iron-Mn nodules containing quartz were also prevalent in all horizons (Figures 5g and 6b, green arrows). These nodules were sometimes altered, resulting in hypocotated features.

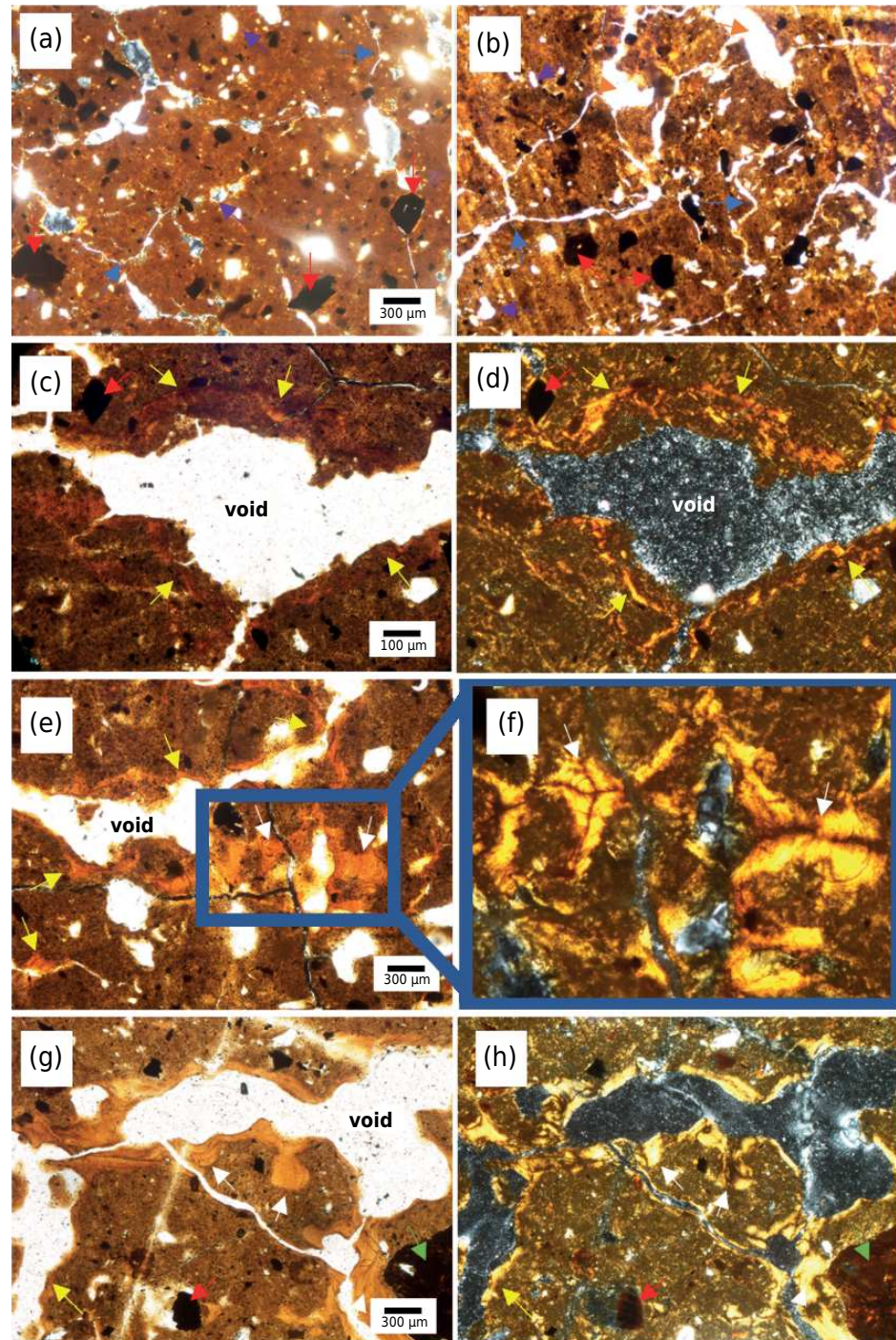


Figure 5. Representative photomicrographs of Bt horizons, highlighting: a and b – block microstructure with planar voids; c and d – monostriated b-fabric associated with clay orientation due to the mechanical expansion and contraction of soil mass; e and f – textural pedofeatures, such as clay coatings and infillings formed by local clay illuviation and deposition; g and h – textural pedofeatures, similar to the previous figures, with striated b-fabric. Photomicrographs in parallel polarized light: a, b, c, e, and g. Photomicrographs in crossed polarized light: d, f, and h. Symbology: blue arrows – planar voids; orange arrows – compound packing voids; purple arrows – vughs; red arrows – ilmenite with alteration (leucoxene) or magnetite with alteration (hematite); yellow arrows – clay orientation with monostriated b-fabric interpreted with a product of mechanical stress by physico-hydric constraints; white arrows – clay coatings or infillings; and green arrows – Fe-Mn-typical nodules.

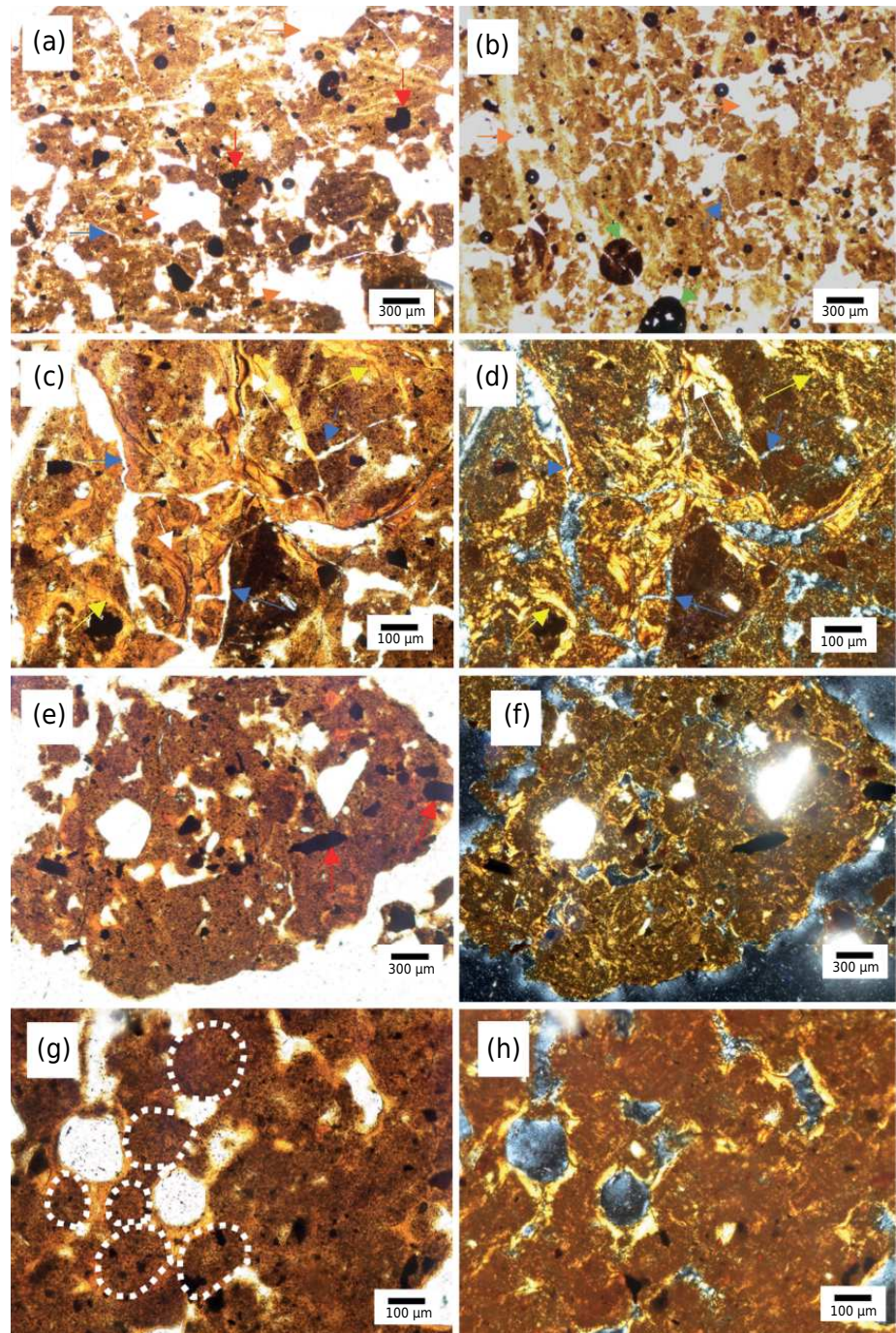


Figure 6. Representative photomicrographs of Bw horizons, highlighting: a and b – block microstructure with planar voids and granular microstructures with compound packing voids; c and d – fragmented textural pedofeatures indicating degradation of them; e and f – sub-rounded block composed by coalesced granules, with granostriated b-fabric in crossed polarized light; g and h – detail of coalesced granules. Photomicrographs in parallel polarized light: a, b, c, e, and g. Photomicrographs in crossed polarized light: d, f, and h. Symbology: blue arrows – planar voids; orange arrows – compound packing voids; purple arrows – vughs; red arrows – ilmenite with alteration (leucoxene) or magnetite with alteration (hematite); yellow arrows – clay orientation with monostriated b-fabric interpreted with a product of mechanical stress by physico-hydric constraints; white arrows – clay coatings or infillings; green arrows – Fe-Mn-typical nodules and white dashed line – granules aggregates.

Soil classification

According to the WRB soil system (IUSS Working Group WRB, 2015), profiles P1 and P4 met all the classification criteria for an argic diagnostic subsurface horizon after the Fe_o/Fe_d ratio <0.05 was excluded from the nitic horizon. Thus, clay was classified as

Lixisol because of the effective base saturation values ($S/Al + S$; IUSS Working Group WRB, 2015) and $CEC < 24 \text{ cmol}_c \text{ kg}^{-1}$. The physical and chemical properties also met the ferralic horizon criteria and the use of the principal qualifier Ferralic, thus confirming advanced weathering. The abundant shiny ped faces of the P1 and P4 profiles allow for the supplementary qualifier Nitic. The highest base saturation in P4 provided the supplementary qualifier Hypereutric, whereas P1 was classified as Ochric.

Profiles P2 and P3 met the classification criteria of a ferralic horizon starting at 1.50 m, and because an argic horizon was found above the ferralic horizon, these soils were classified as Ferralsols. The $Fe_d > 10 \%$ in profile P3 was principally qualified as ferritic, whereas P2 was classified as Haplic. Both profiles had a clayey texture and $V < 50 \%$, and were therefore further classified as Clayic and Dystric (supplementary qualifiers).

Soil taxonomy (Soil Survey Staff, 2014b) was used to classify the soils. All profiles had a moisture regime characterized as Udic with Ochric epipedons. Profiles P1 and P4 were classified as Ultisol and Alfisol, respectively, with argillic horizons due to the blocky structural elements with shiny ped faces. We classified P1 and P4 as Typic Hapludult and Typic Hapludalf, respectively, due to high base saturation. Profiles P2 and P3 met the classification criteria of a Typic Hapludox.

In the Brazilian system of soil classification (*Sistema Brasileiro de Classificação de Solos* – SiBCS; Santos et al., 2018), P1 and P4 were classified as *Nitossolo Háplico* due to the abundance of shiny ped faces, a clayey texture, and monochromatic horizons patterns. In P1, The predominance of base saturation $< 50 \%$ in P1 and $> 50 \%$ in P4 led to their classification as dystrophic and eutrophic, respectively. As in other systems of soil classification, P2 and P3 were classified as *Latossolos Vermelho Amarelo* due to a high degree of weathering. The saturation of base values $< 50 \%$ met the classification of both *Latossolos* as dystrophic.

DISCUSSION

The results suggested that *Nitossolos* was formed by ferralitization and nitidization processes, and then transformed into *Latossolos*, or, in terms of horizons, an argic-ferralic horizon transformation. Evidence for this is discussed below.

Properties of all profiles suggested ferralitization, such as a relative decrease in silicon oxide (SiO_2), increase in $\Delta 4Si\%$, and base content (MgO , CaO , and K_2O) stemming from the increased solubility of these compounds in soil and their removal by leaching (desilication). The $RA\%$, as well as the Fe_2O_3 , Al_2O_3 , TiO_2 , and (MnO) oxide contents increased because of the decreased solubility and/or increased resistance of minerals such as ilmenite ($FeTiO_3$) and rutile (TiO_2) to weathering, (Buol et al., 2011; Dortzbach et al., 2016; Santos et al., 2016a; Camêlo et al., 2017; Kögel-Knabner and Amelung, 2021).

Intensification of the ferralitization process characterizes soils with a high degree of pedogenetic development, culminating in profiles with predominant kaolinite, Fe, and Al oxides in the clay fraction (Santos et al., 2010; Buol et al., 2011; Oliveira et al., 2020; Silva et al., 2020; Kögel-Knabner and Amelung, 2021). Figures 3 and 4 show diffractograms of the clay fraction (iron oxide concentration) in the presence of goethite and hematite in both the Bt and Bw horizons, without a distinction of mineralogical assembly between them. The absence of reflection associated with gibbsite could be due to both the low concentration in the clay fraction (Moore and Reynolds, 1997) and environmental conditions (Melo et al., 2020). According to Camêlo et al. (2017) and (Melo et al., 2020), the high content of organic matter (OM) in the surface horizon and the low Al content (exchangeable) might inhibit gibbsite formation. Another factor is the

competitive isomorphic substitution of Fe by Al in goethite, which is common in these soils (Camêlo et al., 2017; Melo et al., 2020).

The amount of clay imbued all profiles with a clay texture. A hard and firm block structure predominated in approximately 60 % of the horizons analyzed, especially in the Bt horizon. Clayey texture is typical of soils derived from mafic rocks, of which the weathering of primary minerals, such as amphiboles and pyroxenes, favors the formation of clay minerals and iron oxides and hydroxides (Asio and Jahn, 2007; Buol et al., 2011; Dortzbach et al., 2016; Camêlo et al., 2017; Oliveira et al., 2020; Silva et al., 2020; Santos et al., 2021). The concentrations of oxides and kaolinite were also favored by advanced weathering verified by the indices RA% and $\Delta 4\text{Si}\%$ (Table 5). Santos et al. (2021) evaluated weathering and pedogenesis in profiles from gabbro-derived soil located near the study area in Pinheiral. They found that the progressive weathering of pyroxenes and plagioclases resulted in the neoformation of clay minerals such as kaolinite and iron oxyhydroxides, namely goethite and hematite.

Low silt/clay ratios associated with low CEC values also indicate a more advanced weathering stage (Santos et al., 2018). The increase in clay dispersion in the surface horizons evidenced by CF% values, might be due to the high TOC content associated with factors such as pH, CEC, and clay content (Nelson et al., 1999; Fontana et al., 2014). High surface pb values, especially in P2, P3, and P4, suggested compaction, possibly due to anthropic actions and animal traffic in pasture areas. The average density was higher in all Bt horizons in the two profiles (P1 and P4) than in the Bw horizons (1.24 vs. 1.07 Mg m^{-3}), indicating densification. Cooper and Vidal-Torrado (2005) identified pb values of 1.47 – 1.64 Mg m^{-3} in Bt horizons of Nitisol, highlighting the occurrence of densification primarily resulting from microaggregate coalescence and pore clogging by illuviated clay. According to these authors, this densification translates into altered structure and porosity, transforming a granular, into a subangular blocky structure (Cooper and Vidal-Torrado, 2000).

The pH, V%, and TOC contents tended to increase from P1 to P4 owing to solute leaching and concentration effects on the lower third of the slope. The higher CEC values in the surface horizon than in the subsurface in all profiles were due to the addition of OM from the grass root system, biological activity, and nutrient cycling, thus highlighting the importance of the organic fraction for maintaining soil fertility. Furthermore, because of the higher TOC content, the Fe_o values in the surface horizons were higher than those in the subsurface, which can be attributed to iron complexation by functional groups of OM, which decreased iron availability, especially in terms of degrees of oxide crystallinity (Kämpf and Schwertmann, 1983; Maranhão et al., 2016). According to Asio and Jahn (2007), high Fe_d values associated with low Fe_o/Fe_d ratios indicate the predominance of more crystalline oxide forms, such as goethite, and characterize more weathered soils. Inda Júnior and Kämpf (2005) and Ghidin et al. (2006) found that the Fe_o/Fe_d ratio tended to be 0.01–0.05 in soils derived from rocks with a high ferromagnesian mineral content, which corroborated the findings.

The weathering product of ilmenite results from iron dissolution with relative titanium enrichment that results in leucoxene formation (Figure 5) (Deer et al., 1966; Santos et al., 2021). In turn, magnetite weathering through the gradual oxidation of structural Fe^{2+} to Fe^{3+} might lead to hematite formation during pedogenesis in a mineralogical pathway that differs from that of mafic systems, wherein magnetite can be transformed into hematite by oxidation (Santana et al., 2001; Camêlo et al., 2017). Weathering and iron loss were evidenced by hypocointing around both lithogenic oxides (Figure 5). This is only possible because of the slow weathering of magnetite and ilmenite. However, the contribution to the increase in pedogenic iron oxyhydroxides was not significant compared with pyroxene and amphibole weathering.

Santos et al. (2021) evaluated soil from pedogenesis gabbro weathering. They found that some of the iron released from weathered primary minerals such as pyroxenes, amphiboles, and ilmenite under alternating wet and dry conditions (redox potential) might precipitate as ferruginous nodules with a moderate to strong degree of impregnation and sharp, crystalline, and/or slightly crystalline edges. We found nodules in all horizons analyzed (Figures 6, 7, 8 and 9).

Thus, ferralitization was responsible for the genesis of the soil matrix in the studied profiles and their physical, mineralogical, and chemical properties. In addition, nitridation can also explain the appearance of shiny surfaces in the aggregates. These features were abundant in the soils along the toposequence, but were macroscopically evident only in the P1 and P4 profiles, which is why they were classified as *Nitossolos*. Despite the absence of a textural gradient, the abundance of shiny ped faces met the requirements for argic-horizon identification. These features were identified only at the microscopic level in the other profiles, especially in the Bw horizon in the form of grains and pores with moderate-to-strong, parallel, and convoluted orientations coated with clay, as well as complete and incomplete dense infillings with strong parallel orientations.

These textural features are mainly related to clay illuviation but might also be associated with other mechanisms, such as stress constraints or local clay redistribution due to clay dispersion (Cooper and Vidal-Torrado, 2005; Kühn et al., 2010; Buol et al., 2011; Kögel-Knabner and Amelung, 2021; Castro and Cooper, 2019). Clay content in illuvial genesis increases with depth due to vertical translocation favored by the positioning, slope, and landform of the profile, and is deposited in structural units of subsurface horizons (Dortzbach et al., 2016). According to Kögel-Knabner and Amelung (2021), blocky aggregates break up into microstructures with shiny surfaces, resulting from the expansion and contraction of soil mass. Illuvial genesis is the most frequently cited reason, but the physical genesis is very important for the formation of *Nitossolos*, mainly because these soils do not have a textural gradient (Sombroek and Siderius, 1981).

Our results suggested that textural features formed throughout the toposequence, but the nitridation process no longer prevailed. This process is perceptible under field conditions as the macroscopic presence or absence of blocky structures with shiny faces, characterizing Bw and Bt horizons, respectively, and sometimes within the same profile (P1, P3, and P4). However, the micromorphological description best supports these findings.

A block microstructure with planar voids predominated in the Bt horizon (Figures 5a and 5b). In portions with less developed voids and a higher degree of accommodation between them, a striated b-fabric was located at the edges of aggregates, suggesting the orientation of the micromass (Figures 5c and 5d). These features increased as the pores opened, suggesting that their formation followed block fragmentation (Figure 5e). However, the features of coating and void filling along with typical striated b-fabric indicated that in addition to the mechanical processes, clay migrated and became deposited, albeit locally (Figures 5e and 5f). This revealed a mixed origin of the textural features, in which mechanical processes associated with wet and dry cycles and translocation within the same horizon are responsible for their formation.

Microstructures in blocks with clay coatings around aggregates and inside the voids remained in the Bw horizon. However, polyhedral structures fragmented in several portions of the thin sections and formed smaller and more rounded aggregates of typically granular microstructures (Figures 6a and 6b). Some blocks comprised coalesced granules with granostriated b-fabric in cross-polarized light (Figures 6e and 6f). In areas where textural features were thicker, this fragmentation also physically degraded clay coatings (Figures 6c and 6d) (Kühn et al., 2010). This process seemed to lead the oriented clay back to the interior of the micromass of the granular aggregates to some extent,

reducing the textural features and partially transforming the striated, into a granostriated and speckled b-fabric. These micromorphological findings fit the model presented by Pédro et al. (1976) and suggested that after the argic horizon formed, it transformed into a ferralic horizon; that is, the *Nitossolos* transformed into *Latossolos*.

Interplay between *Nitossolos* and *Latossolos* is complex, and each can transform into the other under tropical climatic conditions. The evolution of shiny peds might be a key marker under both circumstances. The results of a study of Ethiopian Nitisol pedogenesis by De Wispelaere et al. (2015) found no support for this hypothesis, in which the development of a Nitisol is related to the subsequent development of Ferralsols. Espíndola (2010) described that a transformation from a ferralic to an argic horizon is normal and considers the process as regressive evolution. Cooper et al. (2010) identified a model of structural transformation through micromorphological findings of a ferralic-to-nitic horizon. This transformation was attributed to natural environmental changes from dry to wet climates, with a well-defined dry season that accounted for more frequent wet and dry cycles. Under these conditions, cracking resulting from the coalesced material generated polyhedral aggregates from the microaggregates.

In contrast, Nakashima (2013) described an argic/nitic-ferralic transformation. These studies also identified a structural model that shows the transformation of one horizon from another. According to these authors, the polyhedral structures of the argic horizon are formed by expansion/contraction, and this movement reorients these structures. More intense dry cycles break the aggregates and form voids, increasing water macroporosity and percolation. This leads to the wear of polyhedral structures, which reorganize into the microaggregates typical of ferralic horizons. Our findings were similar to these.

The evolution of soils in the studied toposequence showed that a pedological system in equilibrium (Bocquier, 1973) that was responsible for the transformation of basic rocks (diabase) into *Nitossolos* was replaced by that of lateral transformation, in which *Nitossolos* are transformed into *Latossolos*. This fact might reflect regional climate changes, with possible attenuation by some local base effects, the contrast between drier and wetter seasons, or even the effects on the dynamics of water movement on the slope, or tectonic influences. The transformation of one soil into another marks a disturbance in the system, and future studies should contribute to elucidating how it is associated with regional landscape evolution.

CONCLUSIONS

The presence or absence of shiny ped faces under field conditions comprises an important marker for the classification of basic rock-derived soils. The most evident pedogenetic processes in the study's location were ferralitization and nitidization due to advanced weathering, the accumulation of oxyhydroxides and kaolinite in the micromass, and the formation of textural pedofeatures caused by mechanical-hydric stress and local illumination. These processes were responsible for the formation of the argic horizon.

Morphological evidence suggested an argic-ferralic horizon transformation. This is supported by the macromorphological absence of shiny ped faces in some horizons (Bw), and their micromorphological coexistence in Bt and Bw horizons within the same profile, and the transformation of the blocky, into the granular microstructure evident on thin sections. The toposequence reflected a lateral *Nitossolo-Latossolo* transformation.

ACKNOWLEDGMENT

To CAPES for awarding fellowships to A. C. Santos; to CPGA-CS, ESALQ/USP e Facultad de Ciencias-UGR and to the Laboratory of Soil Genesis and Classification of the UFRRJ for technical support.

AUTHOR CONTRIBUTIONS







Conceptualization:  Marcos Gervasio Pereira (lead).







Formal analysis:  Marcos Gervasio Pereira (equal) and  Miguel Cooper (equal).

Funding acquisition:  Marcos Gervasio Pereira (lead).

Methodology:  Marcos Gervasio Pereira (lead).

Project administration:  Marcos Gervasio Pereira (lead).

Writing - original draft:  Deyvid Diego Carvalho Maranhão (equal),  Fábio Soares de Oliveira (equal),  Lúcia Helena Cunha dos Anjos (equal),  Marcos Gervasio Pereira (equal),  Miguel Cooper (equal) and  Rafael Cipriano da Silva (equal).

Writing - review & editing:  Deyvid Diego Carvalho Maranhão (equal),  Fábio Soares de Oliveira (equal),  Lúcia Helena Cunha dos Anjos (equal),  Marcos Gervasio Pereira (equal),  Miguel Cooper (equal) and  Rafael Cipriano da Silva (equal).

REFERENCES

- Ab'Saber A. Domínios morfoclimáticos e solos do Brasil. In: Alvarez VVH, Fontes LEF, Fontes MPF, editors. Os solos nos grandes domínios morfoclimáticos do Brasil e o desenvolvimento sustentável. Viçosa, MG: Sociedade Brasileira de Ciência do Solo; 1996. p. 1-18.
- Alvares CA, Stape JL, Sentelhas PC, Gonçalves JLM, Parovek G. Köppen's climate classification map for Brazil. Meteorol Z. 2013;22:711-28. <https://doi.org/10.1127/0941-2948/2013/0507>
- Asio VB, Jahn R. Weathering of basaltic rock and clay mineral formation in Leyte, Philippines. Philipp Agric Sci. 2007;90:204-12.
- Blake GR, Hartge KH. Particle density. In: Klute A, editor. Methods of soil analysis: Part 1 Physical and mineralogical methods. Madison: SSSA; 1986. p. 377-82. <https://doi.org/10.2136/sssabookser5.1.2ed.c14>
- Bocquier G. Génèse et évolution de deux toposéquences de sols tropicaux du Tchad: interprétation biogéodynamique. Bondy: Cah. 0 RS.T.O.M.; 1973.
- Brasil - Projeto Radambrasil. Levantamento de recursos naturais - Folhas SF. 23/24. Rio de Janeiro: IBGE/Ministério das Minas e Energia-Secretaria Geral; 1983.
- Brindley GW, Brown G. Crystal structures of clay minerals and their X-Ray identification. 2nd ed. London: Mineralogical Society; 1980.
- Bullock P, Fedoroff N, Jonguerius A, Stoops G, Tursina T. Handbook of soil thin section description. Wolverhampton: Waine Research Publication; 1985.
- Buol SW, Southard RJ, Graham RC, McDaniel PA. Soil genesis and classification. Soil genesis and classification. 6th ed. Chichester: John Wiley & Sons; 2011.
- Camêlo DDL, Ker JC, Fontes MPF, Corrêa MM, Costa ACS, Melo VF. Pedogenic iron oxides in iron-rich Oxisols developed from mafic rocks. Rev Bras Cienc Solo. 2017;41:e0160379. <https://doi.org/10.1590/18069657rbcs20160379>
- Caner L, Radtke LM, Vignol-Lelarge ML, Inda AV, Bortoluzzi EC, Mexias AS. Basalt and rhyodacite weathering and soil clay formation under subtropical climate in southern Brazil. Geoderma. 2014;235:100-12. <https://doi.org/10.1016/j.Geoderma.2014.06.024>
- Castro SS, Cooper M. Fundamentos de micromorfologia de Solos. Viçosa, MG: Sociedade Brasileira de Ciência do Solo; 2019.
- Comitê para Integração da Bacia Hidrográfica do Rio Paraíba do Sul - CEIVAP. Diagnóstico dos recursos hídricos (Relatório Parcial). In: Plano da bacia do Rio Paraíba do Sul. Rio de Janeiro: Fundação COPPETEC / AGEVAP; 2006. Available from: <https://www.ceivap.org.br/downloads/PSR-006-R0.pdf>

- Cooper M, Vidal-Torrado P. Caracterização morfológica, micromorfológica e físico-hídrica de solos com horizonte B nítrico. *Rev Bras Cienc Solo*. 2005;29:581-95. <https://doi.org/10.1590/S0100-06832005000400011>
- Cooper M, Vidal-Torrado P. Ferriargillan genesis in argillic B horizons of a soil sequence over diabase in Piracicaba. *Sci Agric*. 2000;57:745-50. <https://doi.org/10.1590/S0103-90162000000400024>
- Cooper M, Vidal-Torrado P, Grimaldi M. Soil structure transformations from ferralic to nitic horizons on a toposequence in southeastern Brazil. *Rev Bras Cienc Solo*. 2010;34:1685-99. <https://doi.org/10.1590/S0100-06832010000500021>
- Costa EM, Tassinari WDS, Pinheiro HSK, Beutler SJ, Anjos LHC. Mapping soil organic carbon and organic matter fractions by geographically weighted regression. *J Environ Qual*. 2018;47:718-25. <https://doi.org/10.2134/jeq2017.04.0178>
- De Wispelaere L, Marcelino V, Regassa A, De Grave E, Dumon M, Mees F, Van Ranst E. Revisiting nitic horizon properties of Nitisols in SW Ethiopia. *Geoderma*. 2015;243-244:69-79. <https://doi.org/10.1016/j.geoderma.2014.12.021>
- Deer WA, Howie RA, Zussman J. An introduction to the rock-forming minerals. London: Longman Group Limited; 1966.
- Dortzbach D, Pereira MG, Anjos LHC, Fontana A, Silva Neto EDC. Genesis and classification of soils from subtropical mountain regions of southern Brazil. *Rev Bras Cienc Solo*. 2016;40:e0150503. <https://doi.org/10.1590/18069657rbcs20150503>
- Espíndola CR. A pedologia e a evolução das paisagens. *Rev Inst Geol*. 2010;31:67-92. <https://doi.org/10.5935/0100-929X.20100005>
- Fontana A, Pereira MG, Anjos LHC, Santos AC, Bernini TA. Matéria orgânica de horizontes superficiais em topossequências em ambiente de Mar de Morros, Pinheiral, RJ. *Rev Cienc Agron*. 2014;45:221-9. <https://doi.org/10.1590/S1806-66902014000200001>
- Ghidin AA, Melo VF, Lima VC, Lima JMJC. Oxisol toposequences developed from basaltic rocks in Paraná State, Brazil. I- clay fraction mineralogy. *Rev Bras Cienc Solo*. 2006;30:293-306. <https://doi.org/10.1590/S0100-06832006000200010>
- Hallett RB, Kyle PR. XRF and INAA determinations of major and trace elements in geological survey of Japan igneous and sedimentary rock standards. *Geostand. Geoanalytical Res*. 1993;17:127-33. <https://doi.org/10.1111/j.1751-908X.1993.tb00128.x>
- Inda Júnior AV, Kämpf N. Goethite and hematite variability via reductive dissolution in soils from tropical and subtropical regions. *Rev Bras Cienc Solo*. 2005;29:851-66. <https://doi.org/10.1590/S0100-06832005000600003>
- IUSS Working Group WRB. World reference base for soil resources 2014, update 2015: International soil classification system for naming soils and creating legends for soil maps. Rome: Food and Agriculture Organization of the United Nations; 2015. (World Soil Resources Reports, 106).
- Kämpf N, Schwertmann U. Goethite and hematite in a climosequence in Southern Brazil and their application in classification of kaolinitic soils. *Geoderma*. 1983;29:27-39. [https://doi.org/10.1016/0016-7061\(83\)90028-9](https://doi.org/10.1016/0016-7061(83)90028-9)
- Kämpf N, Schwertmann U. The 5-M-NaOH Concentration Treatment for Iron Oxides in Soils. *Clays Clay Miner*. 1982;30:401-8. <https://doi.org/10.1346/CCMN.1982.0300601>
- Kögel-Knabner I, Amelung W. Soil organic matter in major pedogenic soil groups. *Geoderma*. 2021;384:114785. <https://doi.org/10.1016/j.geoderma.2020.114785>
- Kühn P, Aguilar JA, Miedema R. Textural pedofeatures and related horizons. In: Stoops G, Marcelino V, Mees F, editors. Interpretation of micromorphological features of soils and regoliths. Amsterdam, The Netherlands: Elsevier Science; 2010. p. 217-50. <https://doi.org/10.1016/B978-0-444-53156-8.00011-8>
- Maranhão DDC, Pereira MG, Collier LS, Anjos LHC, Azevedo AC, Cavassani RS. Genesis and classification of soils containing carbonates in a toposequence of the Bambuí Group. *Rev Bras Cienc Solo*. 2016;40:e0150295. <https://doi.org/10.1590/18069657rbcs20150295>
- McKeague JA, Day JH. Dithionite- and oxalate-extractable Fe and Al as aids in differentiating various classes of soils. *Can J Soil Sci*. 1966;46:13-22. <https://doi.org/10.4141/cjss66-003>

- Mehra OP, Jackson ML. Iron oxide removal from soil and clays by dithionite – citrate system buffered with sodium bicarbonate. *Clays Clay Miner.* 1960;5:317-27. <https://doi.org/10.1016/B978-0-08-009235-5.50026-7>
- Melo VF, Oliveira Jr JC, Batista AH, Cherobim VF, Favaretto N. Goethite and hematite in bichromic soil profiles of southern Brazil: Xanthization or yellowing process. *Catena.* 2020;188:104445. <https://doi.org/10.1016/j.catena.2019.104445>
- Meunier A, Caner L, Hubert F, El Albani A, Prêt D. The weathering intensity scale (WIS): An alternative approach of the chemical index of alteration (CIA). *Am J Sci.* 2013;313:113-43. <https://doi.org/10.2475/02.2013.03>
- Moore DM, Reynolds RC. X-ray Diffraction and identification and analysis of clay minerals. Oxford: Oxford University Press; 1997.
- Nakashima MR. Gênese dos Nitossolos Vermelhos férricos na bacia do córrego Miringuava, Maringá-PR [thesis]. São Paulo: Universidade de São Paulo; 2013.
- Nelson PN, Baldock A, Oades JM, Churchman GJ, Clarke P. Dispersed clay and organic matter in soil: their nature and associations. *Soil Res.* 1999;37:289-316. <https://doi.org/10.1071/S98076>
- Nummer AR, Machado R, Dehler NM. Pluton emplacement in a releasing bend in a transpressive regime: the Arrozal granite in the Paraíba do Sul shear belt, Rio de Janeiro. *An Acad Bras Cienc.* 2007;79:299-305. <https://doi.org/10.1590/S0001-37652007000200011>
- Oliveira JS, Inda AV, Barrón V, Torrent J, Tiecher T, Camargo FAO. Soil properties governing phosphorus adsorption in soils of Southern Brazil. *Geoderma Reg.* 2020;22:e00318. <https://doi.org/10.1016/j.geodrs.2020.e00318>
- Pédro G, Chauvel A, Melfi AJ. Recherches sur la constitution et la genèse des Terra Roxa Estruturada du Brésil. *Ann Agron.* 1976;27:265-94.
- Portilho AP, Castro MC, Alves GS, Aguiar NF, Silva MS. Balanço Hídrico para Pinheiral, Rio de Janeiro. *Rev Agrogeoamb.* 2011;3:21-8. <https://doi.org/10.18406/2316-1817v3n22011328>
- Santana GP, Fabris JD, Goulart AT, Santana DP. Magnetite and its transformation to hematite in a soil derived from steatite. *Rev Bras Cienc Solo.* 2001;25:33-42. <https://doi.org/10.1590/S0100-06832001000100004>
- Santos AC, Pereira MG, Anjos LHC, Bernini TA, Cooper M. Genesis of soils formed from mafic igneous rock in the Atlantic Forest environment. *Rev Bras Cienc Solo.* 2016a;40:e0150056. <https://doi.org/10.1590/18069657rbcs20150056>
- Santos AC, Pereira MG, Anjos LHC, Bernini TA, Cooper M, Nummer AR, Francelino MR. Soil genesis and classification in the environment “Mar de Morros” in the mid-valley of the river Paraíba do Sul, RJ. *Rev Bras Cienc Solo.* 2010;34:1297-314. <https://doi.org/10.1590/S0100-06832010000400027>
- Santos AC, Silva RC, Silva Neto EC, Anjos LHC, Pereira MG. Weathering and pedogenesis of mafic rock in the Brazilian Atlantic Forest. *J S Am Earth Sci.* 2021;111:103452. <https://doi.org/10.1016/j.jsames.2021.103452>
- Santos GL, Pereira MG, Lima SS, Ceddia MB, Mendonça VMM, Delgado RC. Landform curvature and its effect on the spatial variability of soil attributes, Pinheiral-RJ/BR. *Cerne.* 2016b;22:431-8. <https://doi.org/10.1590/01047760201622042184>
- Santos HG, Jacomine PKT, Anjos LHC, Oliveira VA, Lumberras JF, Coelho MR, Almeida JA, Araújo Filho JC, Oliveira JB, Cunha TJF. Sistema brasileiro de classificação de solos. 5. ed. rev. ampl. Brasília, DF: Embrapa; 2018.
- Santos RD, Lemos RC, Santos HG, Ker JC, Anjos LHC, Shimizu SH. Manual de descrição e coleta de solo no campo. 7. ed. rev. e ampl. Viçosa, MG: Sociedade Brasileira de Ciência do Solo; 2015.
- Silva SHG, Weindorf DC, Pinto LC, Faria WM, Acerbi Junior FW, Gomide LR, Mello JM, Pádua Junior AL, Souza IA, Teixeira AFS, Guilherme LRG, Curi N. Soil texture prediction in tropical soils: A portable X-ray fluorescence spectrometry approach. *Geoderma.* 2020;362:114-36. <https://doi.org/10.1016/j.geoderma.2019.114136>

Soil Survey Staff. Keys to soil taxonomy. 12th ed. Washington, DC: United States Department of Agriculture, Natural Resources Conservation Service; 2014a.

Soil Survey Staff. Soil survey field and laboratory methods manual. Version 2.0. (Soil Survey Investigations Report No. 51). Washington, DC: United States Department of Agriculture, Natural Resources Conservation Service; 2014b.

Sombroek WG, Siderius W. Nitosols, a quest for significant diagnostic criteria. Wageningen, The Netherlands: International Soil Museum; 1981. p. 11-31. (Annual Report).

Stoops G. Guidelines for the analysis and description of soil and regolith thin sections. Madison: Soil Science Society of America; 2003.

Teixeira PC, Donagemma GK, Fontana A, Teixeira WG. Manual de métodos de análise de solo. 3. ed. rev e ampl. Brasília, DF: Embrapa; 2017.

Yeomans JC, Bremner JM. A rapid and precise method for routine determination of organic carbon in soil. *Commun Soil Sci Plant Anal.* 1988;19:1467-76. <https://doi.org/10.1080/001036288009368027>